JOURNAL OF SOLID STATE CHEMISTRY 71, 490–502 (1987)

Defect Intergrowths in Barium Polytitanates

1. $Ba_2Ti_9O_{20}$

PETER K. DAVIES AND ROBERT S. ROTH*

*Department of Materials Science and Engineering, University of Pennsylvania, Philadelphia, Pennsylvania 19104; and *National Bureau of Standards, Gaithersburg, Maryland*

Received March 18, 1986; in revised form April 17, 1987

Using high-resolution transmission electron microscopy, we have investigated the mechanisms of defect formation in samples of the microwave dielectric material, $Ba_2Ti_9O_{20}$. We found that materials prepared by a variety of different techniques all show considerable structural disorder. The most prevalent intergrowth involved formation of a new triclinic polytype with an ionic arrangement closely related to that in the accepted structure. Defects also resulted from considerable microtwinning and were observed mainly in the samples prepared from a vanadate flux. The degree of nonstoichiometric defect formation was small in comparison to the stoichiometric intergrowths. In this case defects appeared to result from the incorporation of excess vacancies into the close-packed layers of the structure. Barium-deficient surface phases were also formed via a similar mechanism.

1. Introduction

Over the past 10 years several ceramic materials have been developed for incorporation in high-quality microwave-integrated filters (*1, 2*). A suitable ceramic dielectric microwave resonator material must have low loss in the microwave region, a low-temperature coefficient of dielectric constant, and a high dielectric constant, typically 35–40. Most of the research conducted on ceramic dielectric resonators has focused on phases in the $BaO–TiO_2$ system. The two most popular materials, which are manufactured commercially, are $Ba_2Ti_9O_{20}$ and $BaTi_4O_9$. In commercial preparations of $Ba_2Ti_9O_{20}$ several problems have arisen due to variable values for the dielectric loss, Q.

The crystal structure of $Ba_2Ti_9O_{20}$ has recently been determined using single crystal X-ray diffraction (*3*). The structure can be described as a hexagonal close-packed arrangement of barium and oxygen with titanium occupying the appropriate octahedral sites. The pseudo-hexagonal cell has an $(hch)_3$ nine layer stacking sequence with a primitive triclinic cell, $a = 0.7471$ nm, $b = 1.4081$ nm, $c = 1.4344$ nm, $\alpha = 89.94°$, $\beta = 79.43°$, $\gamma = 84.45°$, space group $P\bar{1}$. Figure 1 shows the atomic arrangements in each of the six layers making up the triclinic cell. Two types of barium atoms occur within the layers, half are 12 coordinated by oxygen and the remainder, at $y = 0.25$ and 0.75, are 11 coordinated with a vacancy occurring between the adjacent barium ions. It has been suggested that

0022-4596/87 $3.00

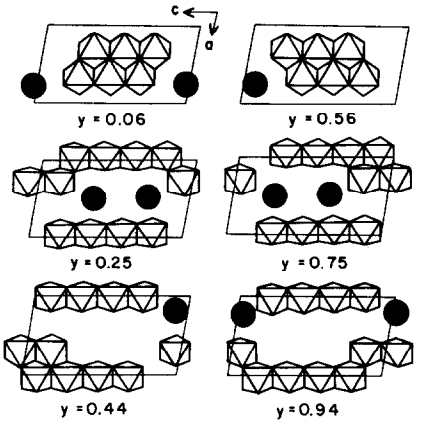

FIG. 1. Atomic arrangements in each of the close-packed layers of the $P\bar{1}$ $Ba_2Ti_9O_{20}$ structure. The large black circles are Ba^{2+} ions, and oxygen positions are represented by the corners of the polyhedra surrounding the Ti^{4+} ions.

the occurrence of the Ba–vac–Ba sequence could be the cause of the superior dielectric properties of $Ba_2Ti_9O_{20}$ as compared to the other barium polytitanates (*4*). However, we note here that both the 6 : 17 and 4 : 13 phases, which do not have outstanding dielectric properties, have more vacancies per (Ba + O) sites than does the 2 : 9 phase.

Two studies of $Ba_2Ti_9O_{20}$ have been made using high-resolution electron microscopy. The first by Grzinic *et al.* (*4*) confirmed the crystal structure also reported by Fallon and Gatehouse (*5*) and described the occurrence of isolated defects. The second study (*6*), published during the course of this work, described defect structures formed in intergrowths of hollandite-"$BaAl_2Ti_6O_{16}$" with $Ba_2Ti_9O_{20}$. Both the previous HREM studies chose to describe the crystal structure of $Ba_2Ti_9O_{20}$ in terms of its relation to hollandite, presumably in part due to their studies being related to the Synroc program. Although certain layers of the structure do bear some resemblance to the hollandite structure, we feel this analogy can be misleading and we retain the more proper description which is in terms of a close-packed structure.

In this paper we report the results of a high-resolution TEM study of $Ba_2Ti_9O_{20}$ ceramics prepared by several different techniques. The investigation was aimed toward studying the defect nature of these materials in order to gain some insight into the variation of the dielectric properties.

2. Sample Preparations

Specimens were examined which had been prepared by several diverse techniques. The majority of the compositions were obtained by heat treatments of powders formed by hydrolysis of metal organic precursors. The technique was fully described by Ritter *et al.* (*7*) and involved preparation of Ba–ethoxide and Ti–ethoxide solutions. These solutions were mixed in a dry argon atmosphere in the desired proportions and then hydrolyzed with or without refluxing by the dropwise addition of 10 : 1 ethanol : water. The precipitate formed was centrifuged, filtered, washed, and dried at 110°C. Heat treatments were performed in Au or Pt crucibles in a $MoSi_2$ box furnace for times ranging from 1 hr to several weeks and at temperatures from ≈500°C to the beginning of melting at ≈1430°C.

Several specimens, typical of the ceramics used for industrial or defense applications at microwave frequencies, were obtained from H. M. O'Bryan of AT&T, Bell Telephone laboratories, and L. P. Dominques of Trans Tech., Inc. These specimens had been fired for various times at temperatures ranging from about 1325 to 1400°C. The heat treatments used in such commercial ceramics generally involved heating and cooling rates of approximately 100°/hr. The powders used for starting materials were usually either $BaCO_3$ or precipitated $BaTiO_3$ and fine-grained TiO_2, probably anatase. A few specimens were also prepared at the National Bureau of Standards using similar conventional solid

state techniques except in special cases (described below). These were pure materials representing equilibrium conditions in the binary system $BaO–TiO_2$. However, the commercial specimens may have contained deliberately (or accidentally) added impurities designed to act as sintering aids or to improve the resultant dielectric properties. Such additions are usually proprietary and no attempt was made to chemically characterize these specimens.

Several specimens examined were prepared at NBS by other techniques involving the use of a third component to aid in the low-temperature formation of the compound $Ba_2Ti_9O_{20}$. As described by Millet *et al.* (*8*) in the phase equilibria study of the ternary system $BaO–TiO_2–V_2O_5$, $Ba_2Ti_9O_{20}$ exists in equilibrium with both $Ba_3(VO_4)_2$ and $Ba_2V_2O_7$. Therefore, a large batch of the 2:9 phase was prepared by mixing $BaTiO_3$ and BaV_2O_6 in a 2:1 molar ratio and heating at 850°C in a Pt crucible. The specimen was removed from the furnace after 3 hr and the resultant partially melted material (the melting point of BaV_2O_6 is ≃708°C) was ground and reheated at 850°C for 18 hr. This material was then boiled in dilute HCl for several hours, washed, and refluxed until the acid remained colorless. This process removed all the $Ba_3(VO_4)_2$ and $Ba_2V_2O_7$, leaving only $Ba_2Ti_9O_{20}$ (with perhaps a trace of TiO_2, rutile). Material derived from this vanadate flux experiment was ultrafine-grained, but crystalline, powder with the characteristic X-ray pattern similar to that of the triclinic $Ba_2Ti_9O_{20}$ heated at much higher temperatures. This powder was then given various temperature and time heat treatments and examined by X-ray and electron diffraction.

As was also shown by Millet *et al.* (*8*), B_2O_3 can be used as a sintering aid to produce dense ceramics of $Ba_2Ti_9O_{20}$ at temperatures as low as 1000°C. One specimen containing 2 mole% addition of B_2O_3 was prepared by the ethoxide precursor technique, hydrolyzed, dried, calcined, pressed into a pellet, and fired at 1000°C for 47 hr. X-ray and electron diffraction showed only $Ba_2Ti_9O_{20}$.

3. Experimental

All the samples used in the HRTEM studies were prepared for microscopy by grinding under acetone and dispersing on holey carbon grids. During the course of the study three different microscopes were used at the University of Pennsylvania, the National Bureau of Standards, and at Arizona State University. These included a Philips 400T, a JEOL 200 CX, and a Philips 430T. Some image calculations were performed using multislice computer programs developed at Arizona State and at Cambridge University (*9*). Extensive simulation of all the structural defects observed in our samples was not attempted and was beyond the scope of this investigation.

4. Results

During the investigation of several samples of $Ba_2Ti_9O_{20}$ prepared by the various techniques described above, many different defects were identified. The major defect, common to all the materials, involved formation of a new polytype of $Ba_2Ti_9O_{20}$ resulting from systematic "stacking faults." A schematic of the projected barium positions in the $P\bar{1}$ structure along the [100] zone axis is shown in Fig. 2. Using this orientation the barium ion arrangement in the stacking sequence can be resolved (see Fig. 3). The most distinctive feature of the arrangement is the "zig-zag" alternation of the Ba–vac–Ba-containing layers at $y = 0.25$ and 0.75. In the normal structure this arrangement is alternately displaced by $+\frac{1}{10}\,c$ and $-\frac{1}{10}\,c$ between each 11 coordinated Ba layer. The correspondence between the image contrast in the nondefective regions and the

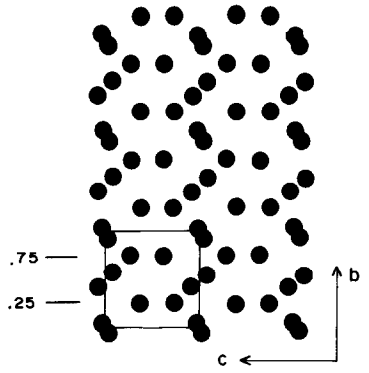

FIG. 2. [100] projection of the barium positions in $P\bar{1}$ $Ba_2Ti_9O_{20}$.

contrast expected from the accepted structure was checked by multislice calculations, and these confirmed that at Scherzer defocus the darker regions in the image faithfully represent the projected Ba positions.

A lattice image of a sample prepared from the orthoethoxide precursors and oriented along the [100] axis is shown in Fig. 4. The micrograph and the corresponding diffraction pattern both indicate that the stacking sequence along *b* is highly disordered. Previous HREM studies (*4*, *6*) had found evidence for isolated defects in this material but the published micrographs do not indicate the high degree of disorder that we have observed in our samples.

The defects in the stacking arrangement are most easily characterized by observing the change in the arrangement of the Ba–vac–Ba sequence. From Fig. 4 it appears that rather than the occurrence of isolated random linear defects, systematic faults lead to the formation of a new polytype. A high-resolution micrograph of one of these regions is presented in Fig. 5. In the new polytype each Ba–vac–Ba-containing layer is regularly displaced by $+\frac{1}{10}$ *c*. The polytype phase formation occurs without any

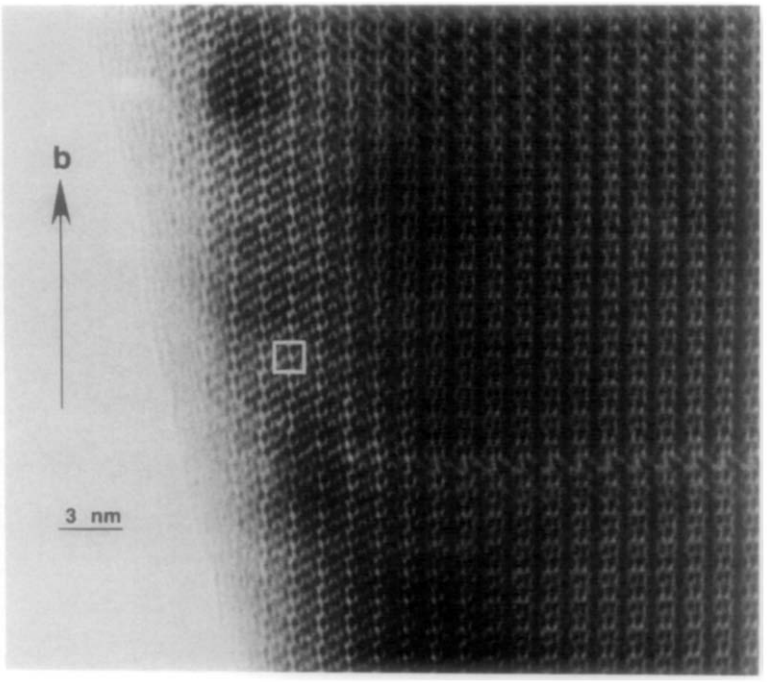

FIG. 3. A [100] high-resolution image of a region almost free of defects. The projected unit cell is outlined.

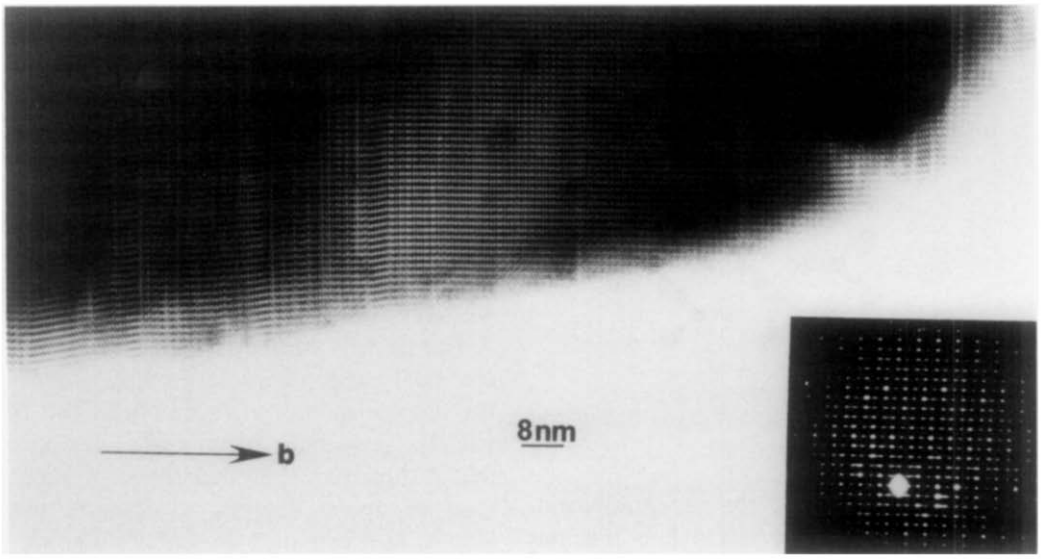

FIG. 4. Lattice image and diffraction pattern collected along [100] showing the occurrence of defects in samples synthesized from orthoethoxide precursors.

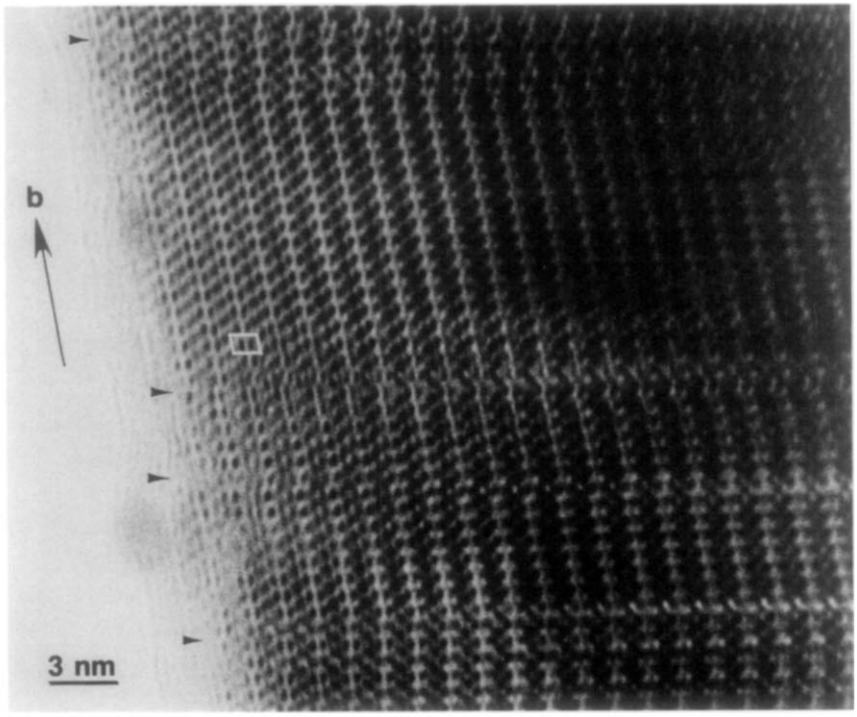

FIG. 5. A high-resolution image of an intergrowth of the $P1$ polytype. Additional defects are arrowed.

change in the overall anion stacking sequence and the mechanism of its formation involves systematic displacement of the Ba ions within the close-packed layers. In Fig. 6 we illustrate the atomic displacements that result in the polytypic transition. For the example shown the intergrowth starts at $y = 0.75$. The Ba–vac–Ba arrangement in the $y = 0.25$ layer is displaced by one atom along c, i.e., by $\frac{1}{5}c$. A corresponding displacement also occurs in the layer below at $y = 0.94$, while the arrangement at $y = 0.06$ is unaffected. Because of the 0.25 displacement the arrangement in the subsequent layer at 0.44 is also displaced by $\frac{1}{5}c$. Similarly the next layer at 0.56 is displaced due to the shift of the following layer at 0.75. The schematic of the projected cell shows the initial and final positions of the barium ions and vacancies.

Each of the barium ion displacements necessarily result in a change in the titanium ion octahedral positions above and below each close-packed layer. Figure 7 shows the new octahedral arrangements resulting from the change in the Ba positions and their relation to the old unit cell.

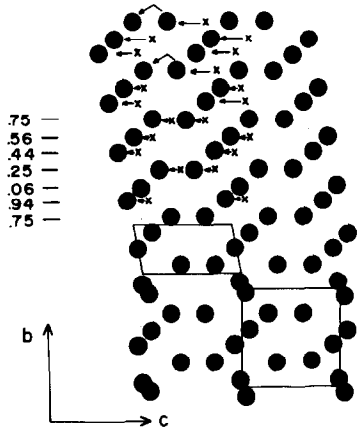

FIG. 6. [100] projection showing the displacement of Ba ions leading to formation of a $P1$ polytype. X represents the position of the ions in the original $P\bar{1}$ structure.

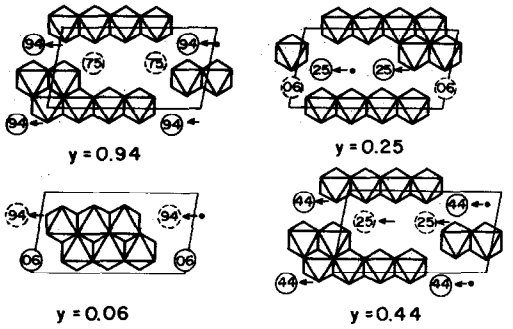

FIG. 7. Rearrangement of the Ti octahedra in the y = 0.94, 0.06, 0.25, and 0.44 layers of the original structure to give the new polytype; the original cell is outlined in each layer.

The Ti positions below the layer at y = 0.94, which was displaced by $\frac{1}{5}c$, become identical to those below the $y = 0.44$ layer in the original structure. The positions below the 0.06 layer, which is not displaced, change as a result of the shift of the 0.94 layer and become equivalent to those below $y = 0.56$ in the original cell. Similarly, the positions below $y = 0.25$ are rearranged because of its displacement relative to 0.06. The octahedra become equivalent to those below 0.75 in the starting structure. The occupancies below 0.44 and 0.56 remain topologically equivalent to those in the starting structure, but are displaced by $\frac{1}{5}c$. The b repeat of the new structure is half that of the original cell and is of reduced $P1$ symmetry, with cell dimensions $a = 0.7471$ nm, $b = 0.7178$ nm, c 1.4344 nm, $\alpha = 78.71°$, $\beta = 79.43°$, and γ = 84.45°. Therefore, the final structure is equivalent to a repeat of half the original cell without its center of symmetry.

In regions of the area shown in Fig. 5 several unit cells of the new polytype can be observed coherently intergrown in the host structure. In all the samples we investigated these polytypic intergrowths were present. However, we noted some variations in the degree of polytypic disorder with the nature of the synthetic pro-

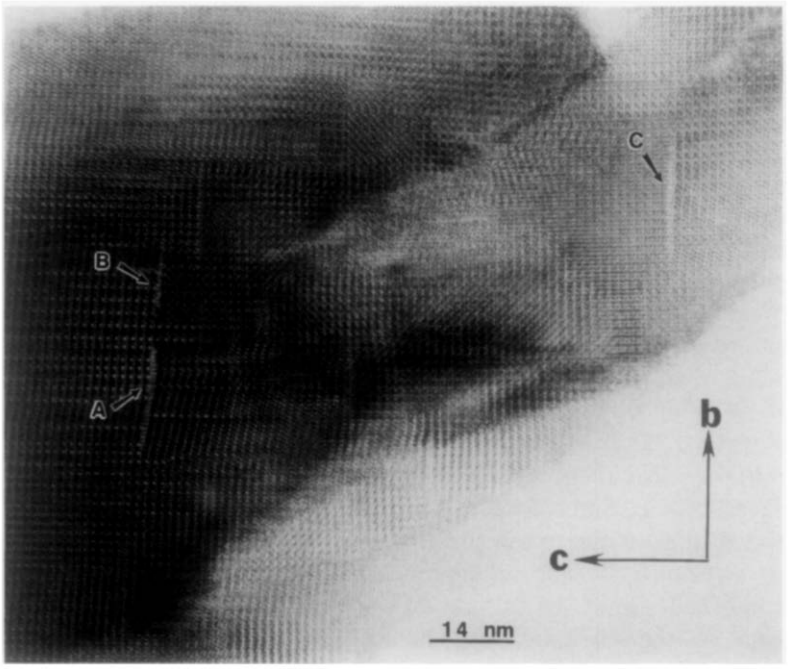

FIG. 8. [100] lattice image of a commercial sample, in addition to the large number of polytypic intergrowths and defects along *b*; in the regions A, B, and C excess vacancies are introduced by intergrowths along *c* (see text and Fig. 12).

cedure. The images shown in Figs. 3–5 were collected from samples prepared from the alkoxide precursors. Although we examined materials which had been sintered at a range of temperatures, we were not able to discern any distinct trends in the degree of disorder as a function of firing temperature. A lattice image collected from a commercial sample of $Ba_2Ti_9O_{20}$ is shown in Fig. 8. In this case it is hard to find any region of the grain that is not massively defective. In addition to the polytypic intergrowths many random stacking faults are present. The diffraction patterns of the grains showed intriguing changes with the degree of polytypic disorder. "Less" defective samples showed only the characteristic streaking along the b^* direction, corresponding to the disorder along the stacking direction. However, as the degree of disorder increased a wave-like modulation could be observed in the c^* direction if the patterns were viewed at an acute angle. Photographs of [100] zone axis patterns viewed at normal and acute angles are shown in Fig. 9.[1] The figure includes a sequence of patterns collected from grains exhibiting increasing amounts of disorder. The amplitude of the modulation increases with the number of defects; finally, in the massively defective commercial samples the patterns become completely incommensurate (see Fig. 9c). These "moire-like" interference effects in reciprocal space result from the random, coherent intergrowth of the two structures at the unit-cell level.

In contrast to the commercial and ethoxide-precursor materials, the samples grown from the vanadate flux were almost

[1] The modulations in the incommensurate diffraction patterns in Fig. 9 have recently been independently modeled by Grzinic (*11*).

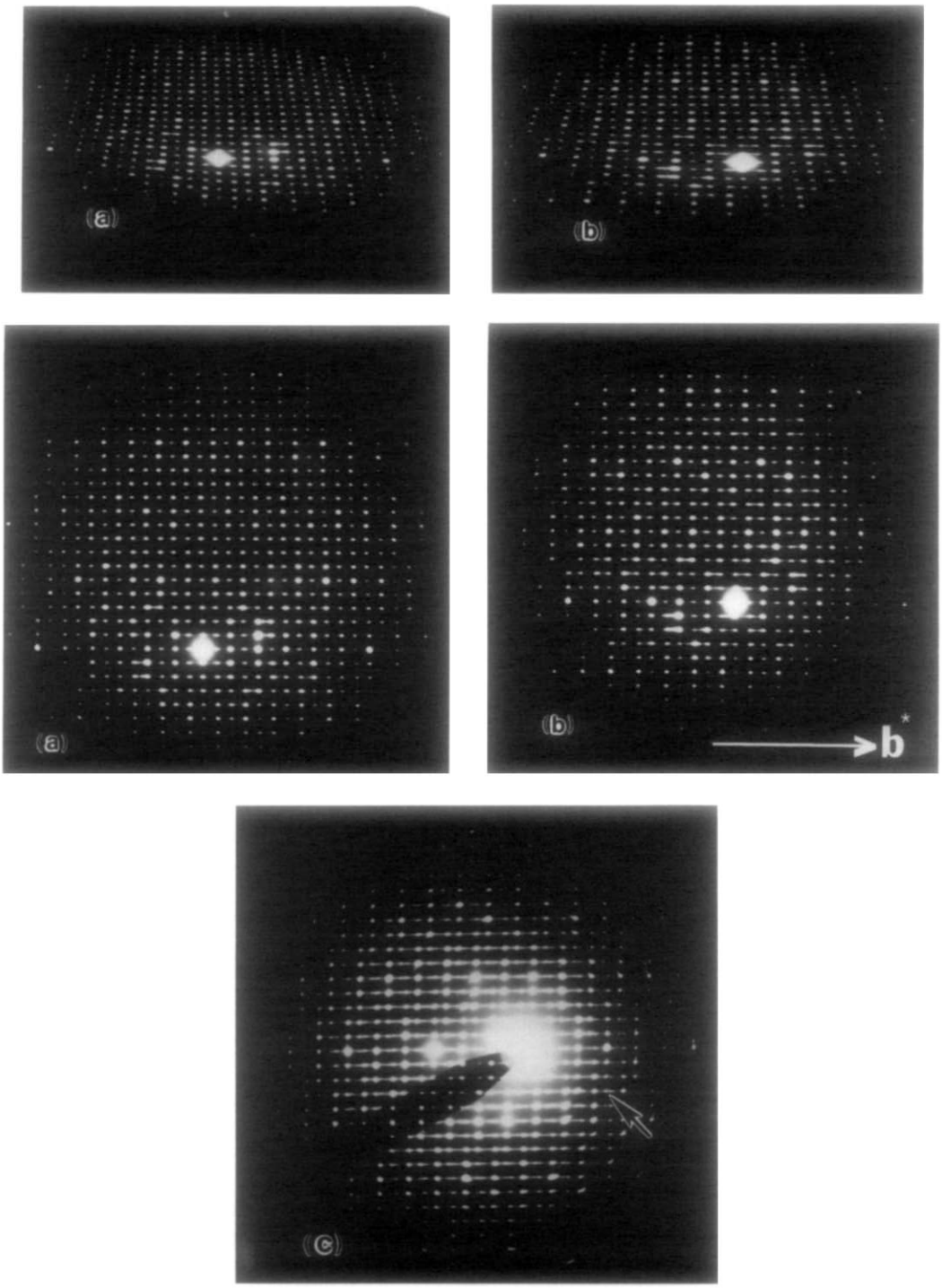

FIG. 9. A series of [100] diffraction patterns collected from samples showing increasing degrees of polytypic disorder. (a) Collected from a region showing only a few defects, (b) from the region shown in Fig. 3. These patterns are also shown at an acute angle to illustrate the sinusoidal modulation along c. (c) An incommensurate pattern collected from a commercial sample.

defect free. In this case we did observe some correlation between firing temperatures and the occurrence of the new polytype. Materials fired at 850°C for 28 hr were noticeably more defective than those fired at 1000 and 1350°C. The higher temperature samples contained very few polytypic intergrowths.

In the case of the main defect mechanism described above, we found no evidence for nonstoichiometry and all the intergrowths appeared polytypic, causing no apparent

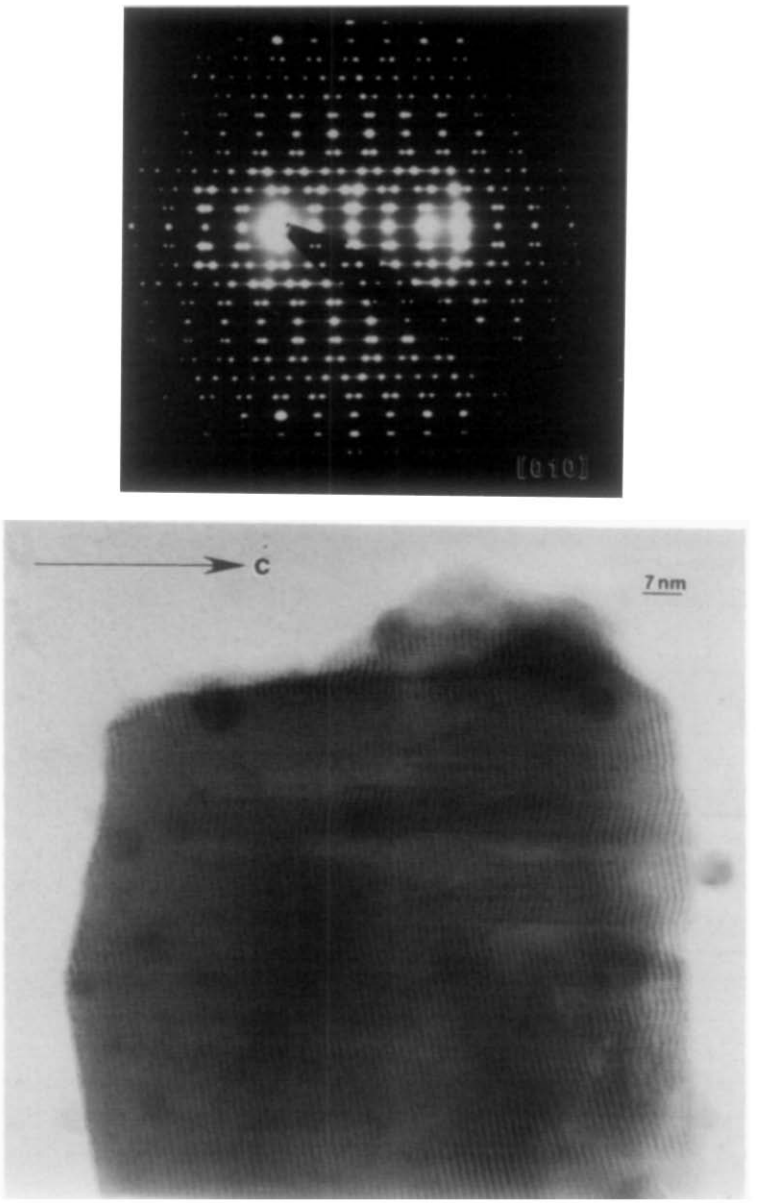

FIG. 10. Twin formation in a sample prepared by the vanadate flux technique.

change in the crystal composition. The second defect observed also appeared to be stoichiometric and resulted in substantial microtwinning of certain samples. Macroscopic twinning in crystals of this structure had been previously observed during a single crystal X-ray investigation (*3*). Indeed a previous structure determination was shown to be in error because of twinned crystals (*10*). The details of the twinning mechanism have not previously been investigated. Figure 10 shows a [010] diffraction pattern and corresponding image collected from a sample prepared from a vanadate flux annealed at 850°C for 28 hr. Both the image and diffraction pattern show evidence for a (100) twin. The interface between the twins appears coherent with no evidence for lattice mismatch or strain. The twin is not a simple reflection twin as this results in an incoherent twin boundary. However, we propose that it can be modeled by the following mechanism involving an inversion twin. The twin is obtained by a displacement of the unit cell by $\frac{1}{2}$ *b* followed by an inversion. A schematic of the atomic arrangements in each of the layers of the new twin and across the twin boundary is given in Fig. 11. Starting with the $y = 0.06$ layer, the ionic arrangement across the boundary changes to that obtained by inverting the arrangement in the layer $y = 0.56$. The layer $y = 0.25$ "twins" with the inversion of $y = 0.75, 0.44$ with inverted 0.94, 0.56 with 0.06, 0.75 with 0.25, and 0.96 with the inversion of 0.44. The resultant twin boundary is coherent and there is no change in the basic packing arrangement. As the image in Fig. 10 shows, the degree of microtwinning in the low-temperature sample is high. As the annealing temperature of the flux-grown crystals was increased the number of twins correspondingly decreased. Some twinning was noted in the commercial materials, but in no other samples was the same degree of twin formation observed. The occurrence

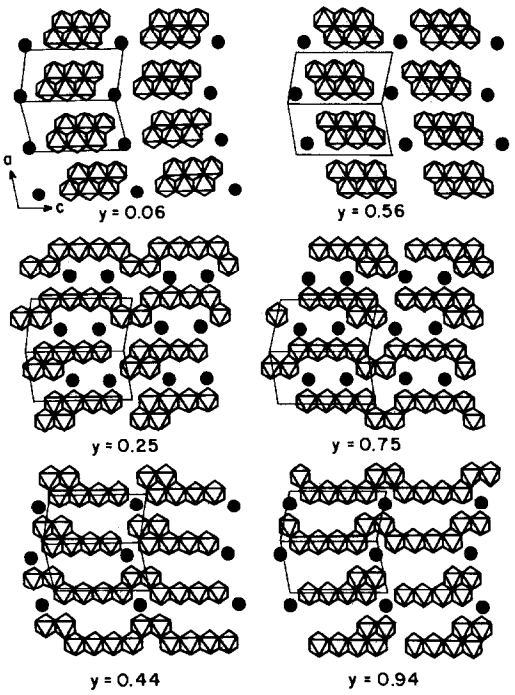

FIG. 11. A schematic model, along [010], for the twin formation in each of the layers of the $Ba_2Ti_9O_{20}$ structure.

of twinning in the flux-grown samples can be rationalized by consideration of the synthetic route. The $Ba_2Ti_9O_{20}$ phase was synthesized from mixtures of BaV_2O_6 and $BaTiO_3$ by solid state flux growth. This technique involves the presence of an initial liquid BaV_2O_6 phase, presumably followed by the growth of nuclei formed from the liquid phase. The nuclei will then grow independently and apparently form several twin boundaries. Subsequent annealing at higher temperatures will result in grain growth and the elimination of many of the twins.

Nonstoichiometric defects were only observed in the commercially prepared ceramics. Referring back to Fig. 8, in which considerable polytypic disorder is observed, in the regions labeled A, B, and C, the contrast variations in the micrograph give evidence for the introduction of excess

vacancies from the intergrowth of adjacent polytypes along (001). In Fig. 12 a region of the sample is shown in which it appears that excess vacancies accommodate the structural disorder in the interface region. This type of defect has been previously reported in work on the $BaO–Al_2O_3–TiO_2$ system. Thus, as shown in the schematic in Fig. 13, the introduction of extra vacancies into the Ba–vac–Ba layers allows the "binding" of the two polytypes intergrown along c and can result in the sequences Ba–vac–vac–Ba, Ba–vac–Ba–vac, Ba–vac–Ba–vac–vac–Ba, and Ba–vac–Ba–vac–Ba–vac–Ba, etc. The lengthening of this sequence necessarily requires the insertion of extra edge-shared titania octahedra into each layer of the structure. For the Ba–vac–vac–Ba sequence this would change the stoichiometry from $Ba_2Ti_9O_{20}$ to $Ba_2Ti_{11}O_{24}$ (see Fig. 13).

A related defect was also observed at the edges of grains of the same sample. For example, in Fig. 14 the extra contrast due to the (010) lattice fringes is lost toward the edge of the grain. Microdiffraction patterns from this region confirmed the loss of this periodicity and tilting experiments confirmed the change in contrast was not an artefact due to poor alignment of the crystal. Judging from the reduced contrast in the micrograph, and by comparison to the

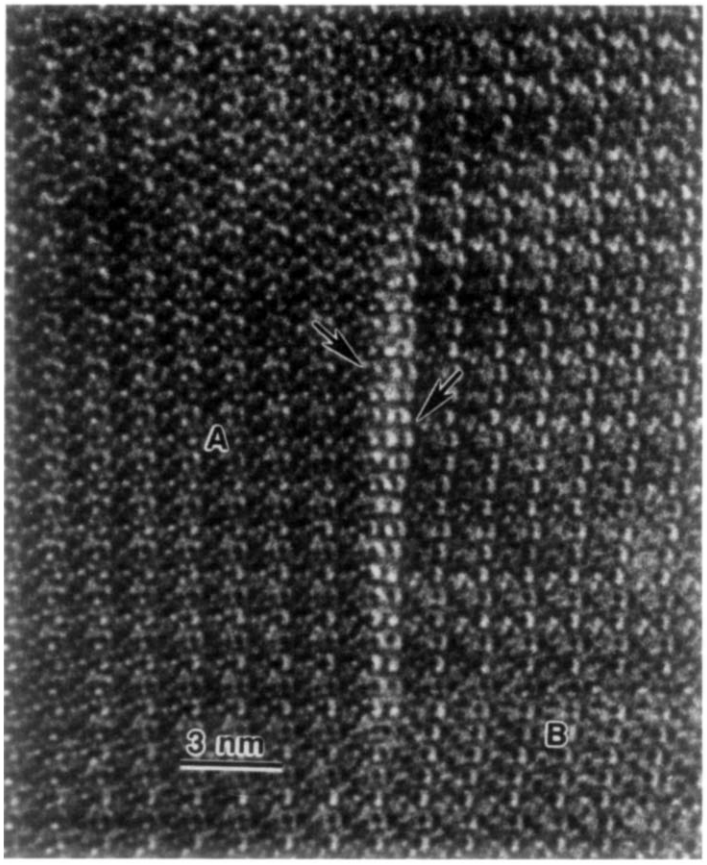

FIG. 12. Excess vacancy formation in a commercial sample. Region A is the defect-free $P\bar{1}$ structure, and region B is primarily the $P1$ polytype.

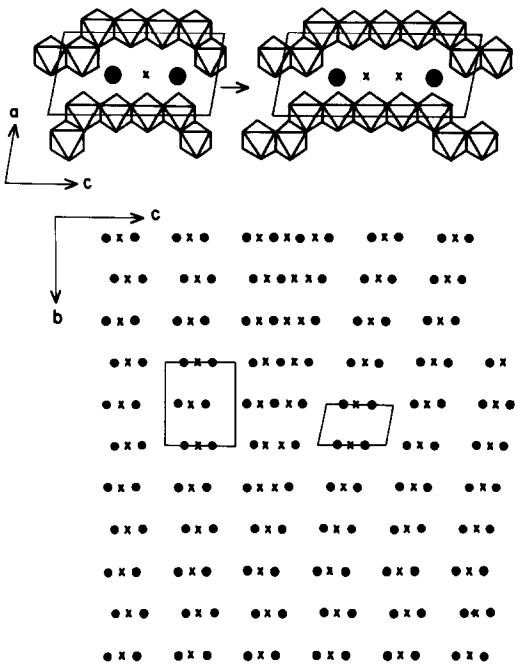

FIG. 13. A schematic of the mechanism for excess vacancy formation. Black circles represent the projected 11-coordinated barium ions, X represents the vacancies between them. For clarity all other ions have been omitted. Also shown is an example of the insertion of extra edge-sharing Ti octahedra that are required to form the excess vacancies.

small excess vacancy defects in the bulk of the grain, we suggest the surface region is barium deficient and may result from extended rows of vacancies within the Ti–O framework. Small amounts of Mn added as sintering aids in the commercial syntheses may aid in the formation of these Ba-deficient phases at the surface, and perhaps in grain boundary regions.

5. Discussion

All the samples of $Ba_2Ti_9O_{20}$ investigated during this work have shown evidence for considerable structural inhomogeneity. By far the most prevalent defect mechanism involves polytypic intergrowth of a structure closely related to that previously determined by X-ray techniques. The degree to which the samples were intergrown appeared to be dependent on both the synthetic technique and the final annealing temperature. For example, crystals grown from a vanadate flux showed less polytypism than samples synthesized from orthoethoxide precursors which in turn are less defective than commercial materials grown by conventional solid state techniques. At this stage the reasons for these differences are unclear. We had hoped to correlate the degree of polytypism with the firing temperature. This proved not to be possible with either the orthoethoxide or commercial samples mainly because the samples were so defective that "counting" defects was not feasible. Some evidence was obtained for a decrease in the number of defects with increasing temperature in the vanadate flux materials.

By comparison to the polytypic defects, nonstoichiometric defects do not seem to play a major role in our specimens. Significant degrees of nonstoichiometry were only observed in the commercial samples, and excess vacancies were present both in the bulk of the grains and also at the edges of some grains. These, together with the large number of interface regions between the polytypic defects, may be very significant in controlling the dielectric loss properties of these ceramics. It is clear that it is extremely difficult to reach equilibrium conditions in this system and produce a defect-free structure. The situation is probably complicated by barium loss and titanium oxidation/reduction phenomena at higher temperatures. One of the original aims of this work was to explain the poorly understood variations in the dielectric loss. As described above, because the materials are so defective it is difficult to give any quantitative explanation for the variations in the loss, but it does seem likely that they result from different degrees of polytypic intergrowth. In order to give a more quantitative explanation it will be necessary to perform dielectric measurements on samples with widely differing degrees of

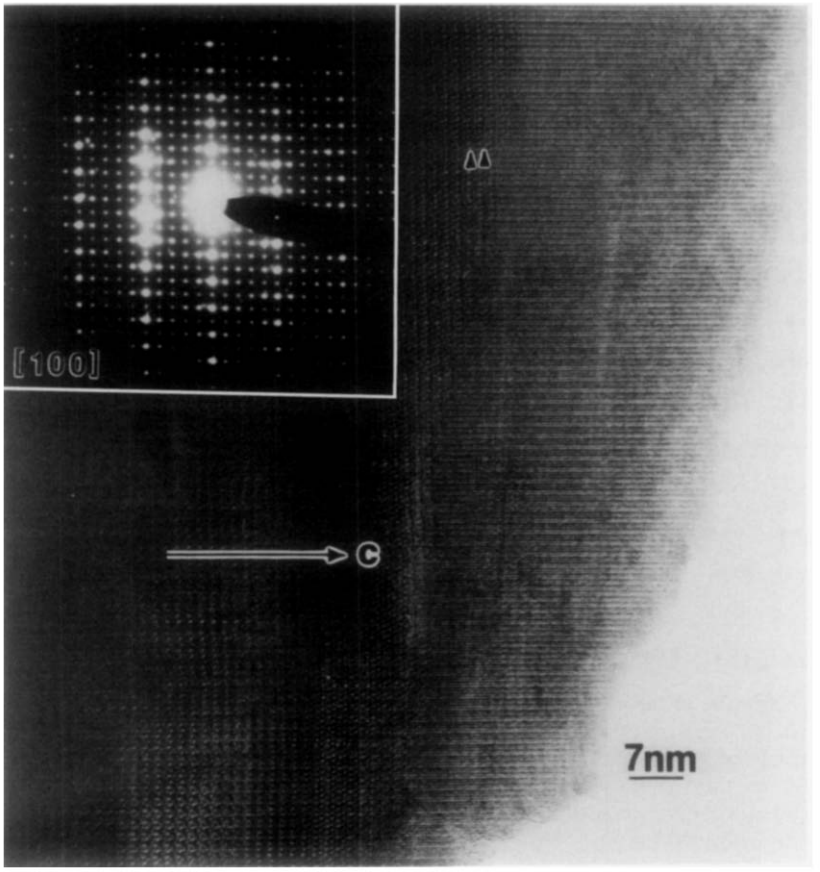

FIG. 14. A [100] high-resolution image of barium-deficient surface phases in commercial samples of $Ba_2Ti_9O_{20}$. The contrast corresponding to the long repeat along c is lost toward the edge of the grain.

disorder. Preparation of materials with substantial disorder is not difficult, and the most promising method for preparation of defect-free samples appears to be via the vanadate flux growth method.

Acknowledgments

This work was supported by NSF—Solid State Chemistry—Grant DMR 831699 (P.K.D.). Use of facilities provided under NSF (MRL) Grant DMR 8216718 (P.K.D.) is also acknowledged.

References

1. J. K. PLOURDE, D. F. LIN, H. M. O'BRYAN, JR., AND J. THOMSON, JR., *J. Amer. Ceram. Soc.* **58,** 418 (1975).
2. H. M. O'BRYAN, JR., J. THOMSON, JR., AND J. K. PLOURDE, *J. Amer. Ceram. Soc.* **57,** 450 (1974).
3. E. TILLMANNS, W. HOFMEISTER, AND W. H. BAUR, *J. Amer. Ceram. Soc.* **66,** 268 (1983).
4. G. GRZINIC, L. A. BURSILL, AND D. J. SMITH, *J. Solid State Chem.* **47,** 151 (1983).
5. G. D. FALLON AND B. M. GATEHOUSE, *J. Solid State Chem.* **49,** 56 (1983).
6. A. PRING, D. A. JEFFERSON, AND J. M. THOMAS, *J. Solid State Chem.* **55,** 125 (1984).
7. J. J. RITTER, R. S. ROTH, AND J. E. BLENDELL, *J. Amer. Ceram. Soc.* **69,** 155 (1986).
8. J. M. MILLET, R. S. ROTH, AND H. PARKER, *Commun. Amer. Ceram. Soc.* **69,** 103 (1986).
9. M. A. O'KEEFE AND P. R. BUSECK, *Trans. Amer. Crystallogr. Assoc.* **15,** 27 (1979).
10. H. M. O'BRYAN, W. H. GRODKIEWICZ, AND J. L. BERNSTEIN, *J. Amer. Ceram. Soc.* **63,** 309 (1980).
11. G. GRZINIC, *Phil. Mag. A* **52,** 161 (1985).